Prediction method for tire air-pumping noise using a hybrid technique

Sungtae Kim[a)]
School of Mechanical and Aerospace Engineering, Seoul National University, Building 301-1214, Seoul 151-742, Korea

Wontae Jeong[b)]
Applied Technology Research Department, Hyundai MOBIS, 80-10, Mabook-Dong, Giheung-Gu, Yongin-Shi Gyunggi-Do 449-910, Korea

Yonghwan Park[c)]
School of Mechanical and Aerospace Engineering, Seoul National University, Building 301-1214, Seoul 151-742, Korea

Soogab Lee[d)]
Institute of Advanced Aerospace Technology, School of Mechanical and Aerospace Engineering, Seoul National University, Building 301-1303, Shilim-Dong, Gwanak-Gu, Seoul 151-742, Korea

(Received 22 September 2005; revised 8 February 2006; accepted 5 April 2006)

Air-pumping noise from a car tire is investigated with a hybrid technique composed of three stages: (1) small-scale air-pumping noise generation process is modeled as a piston-like movement of the base-side of the tire groove and then numerically simulated; (2) the flow properties in the tire groove are used as air-pumping sources and noise propagation is simulated with emphasis placed on scattering process with full tire/road geometry; (3) the far-field acoustic pressure is predicted from a Kirchhoff integral method by using unsteady flow data in space and time which is provided by the computational fluid dynamics (CFD) calculation of full tire-road domain. The comparison of predicted results shows that the nonlinearity of the air-pumping noise generation mechanism affects not only noise characteristics in frequency domain but also in the directivity pattern. It seems that this approach can overcome the weakness of the acoustic monopole theory which stems from the usual assumption of a small amplitude acoustic wave equation while using nonlinear governing equation for the CFD calculation. Furthermore, through the use of a computational domain which covers tire and road surface, the geometric effects on air-pumping noise generation and propagation are taken into account in the source modeling process. © *2006 Acoustical Society of America.* [DOI: 10.1121/1.2200140]

PACS number(s): 43.50.Lj, 43.50.Ed, 43.55.Ka, 43.28.Ra [DKW] Pages: 3799–3812

I. INTRODUCTION

In general, tire/road noise generation mechanisms can be divided into vibration-related and aerodynamically-related groups according to the media in which noise occurs and its effects.[1] The examples of the noise of vibration-related mechanism are tread impact noise, texture impact noise and stick/slip or stick/snap noise which result from the impact of tire tread blocks or pattern elements on the road surface, the stroke of road surface texture on the tire tread, and the tread element motion relative to the road surface, respectively. On the other hand, turbulence noise around rolling tire and air-pumping noise caused by the air displacement into/out of cavities in or between the tire tread and the road surface are classified as the noise of aerodynamically-related mechanism. Moreover, pipe resonance in the grooves of tire tread pattern and Helmholtz resonance in the tire tread and the road surface can be categorized into the aerodynamically-related mechanism as a special case of the air-pumping mechanism.[2]

Since the first investigation of the air-pumping noise generation mechanism by Hayden[3] in 1971, most studies have characterized the air-pumping noise source as the volume change of air cavities in car tires. Besides, it has been assumed that the air displaced from the compressed groove feeds an acoustic monopole. In these approaches, the Euler equations are applied for an air-pumping noise source which is modeled as vibrating point monopole source. Here, the sound pressure is related to the second derivative of the volume changes of the squeezed cavities. Until now, lots of studies based on the monopole theory have been performed and some experimental investigations have shown satisfactory agreement with this approach.[4,5]

However, the monopole theory has an intrinsic weakness because it assumes small amplitude fluctuations of pressure and density in the tire groove or around the tire/road contact points for using linearized governing equations. Although

[a)]Electronic mail: yelorei7@snu.ac.kr
[b)]Electronic mail: wtjeong@mobis.co.kr
[c)]Electronic mail: qwer1104@snu.ac.kr
[d)]Author to whom correspondence should be addressed. Electronic mail: solee@plaza.snu.ac.kr

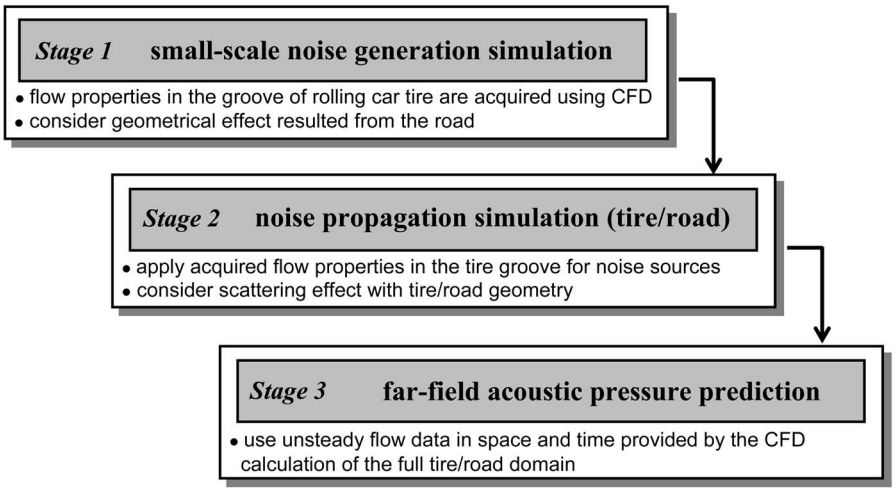

FIG. 1. Schematic diagram of the prediction procedure for the air-pumping noise (combined CFD/Kirchhoff method).

this approach models the air movement as a piston motion moving upward and downward in the cavity, it equates local air movements exactly with the volume changes of the cavity. In the monopole theory, therefore, the movement of the piston does not cause any compression or expansion of the adjacent air. As a consequence, the piston applied in the monopole theory is not directly related with the air-pumping noise generation but is a simple apparatus for the volume changes of the cavity.

Gagen[6] argued that, considering a typical period over which a cavity undergoes squeezing, the volume decrease of the cavity may occur before the air is able to fully evacuate from it. Furthermore, the volume loss of the cavity can cause potentially large density fluctuation. Thus, this invalidates the use of the usual acoustic wave equation which is based on the assumption of small amplitude fluctuation. In order to consider this nonlinear effect, he derived a "squeezed acoustic wave equation" suitable for application to squeezed fluid systems. He considered tire grooves in a rectangular geometry and used the Euler equations for fluid flow together with the moving boundary conditions specifying the cavity under compression. By obtaining an approximate analytic solution, he demonstrated that the usual assumption of the small amplitude acoustic wave equation and the acoustic monopole theory derived from this equation is incorrect for the squeezed system.

However, even in the derivation of the squeezed acoustic wave equation, geometrical effects on the air-pumping noise generation and propagation are not considered. In that the squeezed system doesn't have any wall boundary condition to take into account the contact road surface near the cavity exit, the compressed air may evacuate from the cavity during the whole period of the compression process. In real compression process of the air-pumping mechanism, however, due to the time delay between the volume changes and resultant air movement, some portion of compressed air may be trapped in the cavity. After that, as the cavity moves away from the contact patch, the trapped air is pressed away at the beginning of expansion process and interrupts suction of outside air into the cavity. (Several researchers modeled this noise generation mechanism as a Helmholtz resonance phenomenon, and investigated separately from the air-pumping mechanism.[7,8] Under the consideration of an air-pumping mechanism with the compressible flow properties, however, Helmholtz resonance phenomenon must not be separated.) Besides, when the cavity undergoes compression or expansion (volume decrease or recovery) process, the tire and the road surface form exponentially widening acoustic "horn" geometry close to the leading and trailing edges of the contact patch. And this horn geometry helps to radiate the generated noise and amplifies far-field noise amplitude. Obviously, the variations of these external boundary conditions may change the flow properties in the cavity. As a result, the generation mechanism and the propagation characteristics of the air-pumping noise are different from those of single squeezed system. Therefore, to examine the main features of the air-pumping noise and to find the hidden noise generation mechanism, the air-pumping noise source model and the noise prediction method which can consider the nonlinear noise generation and the geometrical scattering are needed.

In this article, a new method to predict the air-pumping noise in a rolling tire is proposed. This method is based on a hybrid technique which combines a computational fluid dynamics (CFD) technique with a Kirchhoff integral method. First, a Navier-Stokes finite volume solver is executed to solve the squeezed cavity system, which is newly modeled with piston/sliding-door/cavity geometry. Then the resultant flow properties in the grooves of the rolling tire are transferred to the flow simulation of the full tire/road domain as an air-pumping noise source. Finally, in order to predict the far-field acoustic pressure, the flow properties around the rolling tire and the road surface are transferred to the linear Kirchhoff integral method. Figure 1 summarizes the schematic of the proposed prediction procedures.

The outline of the remainder of this article is as follows. First the procedure of the proposed air-pumping noise prediction method is introduced in Sec. II, and numerical formulation is employed follow in Sec. III. The predicted results are provided in Sec. IV, which includes discussions about air-pumping noise generation mechanism in time and frequency domains. In Sec. V, the effect of ventilation on the air-pumping noise is investigated, and predicted results are compared with previous experimental data. The conclusion of this work is then presented in Sec. V.

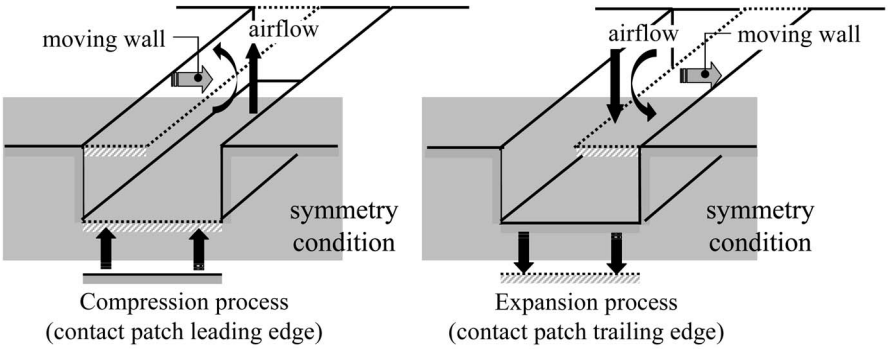

FIG. 2. Schematic diagrams of the piston/sliding-door/cavity source model and boundary conditions of the small scale noise generation simulation.

II. PREDICTION METHOD FOR THE AIR-PUMPING NOISE

A. Small-scale noise generation simulation with the piston/sliding-door/cavity model

When a tire rolls, a tire groove is squeezing as it enters the contact patch between the tire groove and the road surface. As the tire groove progresses through the contact patch, it closes up which results in the air which is trapped within it being compressed. After that, as the tire groove has been released from the contact patch, this compressed air is released and pressed away from it. This squeezing and releasing process of the tire groove is similar to that of pumping noise and known as air-pumping noise generation process.[2]

In the present study, to model this air-pumping noise generation process with considering the effect of the road surface, the piston/sliding-door/cavity model is proposed. The tire groove is modeled as a hexahedral cavity, which has a baffled cavity-cover that acts as a sliding-door and a base-side that moves like a piston. This model is shown schematically in Fig. 2. The squeezing/releasing and resulting volume decreasing/increasing process of the tire groove is modeled by the piston-like movement of the base-side of the cavity. In addition, the relative motion of the contact patch to the tire groove is modeled as the closing/opening motion of the sliding-door at the cavity open end, which has the same period as the compression/expansion motion of the piston. Here, it is assumed that there are no more volume decrease of the tire groove after the tire groove is fully covered by the road surface. Therefore, at the moment that the hexahedral cavity is closed by the sliding-door, the piston is paused and kept in its position for some time period which is determined by the tire rolling speed. After that, as the tire groove moves away from the contact patch trailing edge, the opening motion of the sliding-door and the expansion motion of the piston are started.

B. Near-field noise propagation simulation with the full tire/road geometry

The unsteady flow data obtained in the previous stage are used as air-pumping noise sources in the second stage, where noise propagation is simulated with emphasis placed on the scattering process with the full tire/road geometry. The flow properties in the compression process of the base-side piston are used as an air-pumping noise source in the volume decreasing process of the tire groove at the contact patch leading edge. Also, the properties in the expansion process are used as a noise source in the volume increasing process at the contact patch trailing edge. The schematic diagram of the full tire/road geometry and boundary conditions for the near-field noise propagation simulation are shown in Fig. 3.

In the present study, it is assumed that the tire has a cylindrical geometry. Moreover, the deformation of the tire side-wall is not considered. Thus, the full tire/road geometry has the same conceptual configuration as "the undeformed slick-treaded tyre model" in the TINO project.[9] In order to take into account the tire rolling motion, the angular velocity of the tire is imposed for the wall boundary condition of the cylinder, and the traveling speed of the tire is imposed for the wall boundary condition of the road surface. Further, at the nearest cells to the edges of the contact patch, the air-pumping noise sources are located as line sources. These source terms are determined by the mass flow rate and velocity vector data at the cavity open end, which are acquired in the numerical simulation of the piston/sliding-door/cavity model. The resulting source terms are then added to the governing equations.

C. Far-field acoustic pressure prediction from a Kirchhoff integral method

A linear Kirchhoff integral method is applied to predict the air-pumping noise of a rolling tire. The near-field flow

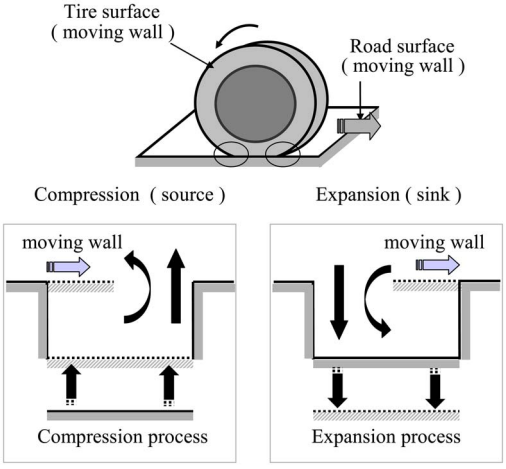

FIG. 3. (Color online) Schematic diagrams of the full tire/road geometry and boundary conditions of the near-field noise propagation simulation.

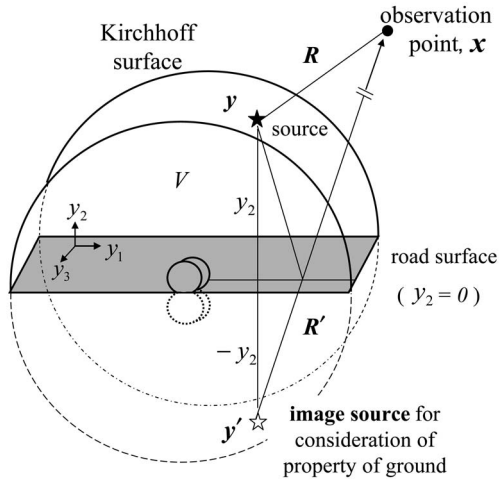

FIG. 4. Schematic diagram of the Kirchhoff surface for the prediction of the air-pumping noise and the coordinate system for half space Green's function (method of images)

data obtained by the CFD calculation of the full tire/road domain with modeled air-pumping noise sources are used as an input to the Kirchhoff integral formula. In order to obtain the coordinate system which is coincident with that of general laboratory road-wheel facility test,[4] the traveling speed of the tire is imposed for the wall boundary condition to the road surface. In this coordinate system, the tire position and the observation point become fixed in space. As a result, the Kirchhoff integral formula for a stationary control surface is acceptable. Then, this Kirchhoff integral formula can be regarded as the analytic expression of Huygens' principle.[10]

The integration is performed at the control surface, called the Kirchhoff surface, containing the flow field information. In the proposed method, the cylindrical surface that is magnified the tire surface can be considered as the control surface. Furthermore, in order to consider reflection effect by the road surface, the method of images[11] is applied by imposing the image sources under the road surface. Figure 4 shows the schematic of the image source and the Kirchhoff surface under the consideration.

III. NUMERICAL FORMULATION

A. Monopole theory

Though the monopole theory is not used in the proposed method, the authors will briefly introduce the monopole theory for later comparison with the proposed method.

The monopole theory applies the acoustic wave equation to a vibrating point source modeled as a small spherical emitter of radius, a, undergoing small oscillations much less than the radius. In case of a spherical wave centered at the coordinate origin, all the flow parameters are functions of the radial distance, r, and t only. Since the pressure gradient acts radially, the fluid velocity can only be in the radial direction. Thus, the wave equation reduced to

$$\frac{1}{c^2}\frac{\partial^2 p'}{\partial t^2} = \frac{1}{r^2}\frac{\partial}{\partial r}\left(r^2\frac{\partial p'}{\partial r}\right), \tag{1}$$

and the general solution of Eq. (1) is as follows:

$$p'(r,t) = \frac{f(r-ct)}{r}, \tag{2}$$

where c is speed of sound, and f can be any functions.

Suppose that the radial velocity at radius, a on the surface of the spherical radiator is specified to be u_a. And, if the source is much smaller than the wavelength of sound, this surface vibration will generate the centered wave like

$$p'(r,t) = \frac{a^2}{r}\rho_0\frac{\partial u_a}{\partial t}\left(t - \frac{r-a}{c}\right), \tag{3}$$

where, ρ_0 is the density of air.

Meanwhile, the resulting volume change is related to the radial velocity on the surface of the sphere taken on the following form:

$$\frac{\partial V}{\partial t} = 4\pi a^2\frac{\partial a}{\partial t} = 4\pi a^2 u_a. \tag{4}$$

In turn, this allows us to substitute Eq. (4) back into Eq. (3) to obtain

$$p'(r,t) = \frac{1}{4\pi r}\rho_0\frac{\partial^2 V}{\partial t^2}\left(t - \frac{r-a}{c}\right), \tag{5}$$

which is relating the pressure wave emitted by a monopole source to the second derivative of the volume change of that source.[12]

B. CFD techniques

An unsteady, compressible, and three-dimensional Navier-Stokes equation is solved to analyze the flow field around a rolling tire and in the squeezed cavity system modeled as the piston/sliding-door/cavity geometry. The system of equations consists of a local time derivative term, three convective, and three viscous flux vectors. In physical coordinates, the governing equation written in the nondimensionalized conservative form is

$$\frac{\partial \mathbf{Q}}{\partial t} + \frac{\partial \mathbf{E}}{\partial x} + \frac{\partial \mathbf{F}}{\partial y} + \frac{\partial \mathbf{G}}{\partial z} = \frac{1}{\mathrm{Re}}\left(\frac{\partial \mathbf{E}_v}{\partial x} + \frac{\partial \mathbf{F}_v}{\partial y} + \frac{\partial \mathbf{G}_v}{\partial z}\right), \tag{6}$$

where conservative variables, $\mathbf{Q}$, and flux vectors are

$$\mathbf{Q}=\begin{pmatrix}\rho\\ \rho u\\ \rho v\\ \rho w\\ \rho e\end{pmatrix},\quad \mathbf{E}=\begin{pmatrix}\rho u\\ \rho u^2+p\\ \rho uv\\ \rho uw\\ (\rho e+p)u\end{pmatrix},$$

$$\mathbf{F}=\begin{pmatrix}\rho v\\ \rho uv\\ \rho v^2+p\\ \rho vw\\ (\rho e+p)v\end{pmatrix},\quad \mathbf{G}=\begin{pmatrix}\rho w\\ \rho uw\\ \rho vw\\ \rho w^2+p\\ (\rho e+p)w\end{pmatrix},$$

$$\mathbf{E}_v=\begin{pmatrix}0\\ \tau_{xx}\\ \tau_{xy}\\ \tau_{xz}\\ (e_v)_5\end{pmatrix},\quad \mathbf{F}_v=\begin{pmatrix}0\\ \tau_{yx}\\ \tau_{yy}\\ \tau_{yz}\\ (f_v)_5\end{pmatrix},\quad \mathbf{G}_v=\begin{pmatrix}0\\ \tau_{zx}\\ \tau_{zy}\\ \tau_{zz}\\ (g_v)_5\end{pmatrix}.$$

With the perfect gas assumption for the Newtonian fluids, shear stress can be written as

$$\tau_{ij}=\mu\left(\frac{\partial u_i}{\partial x_j}+\frac{\partial u_j}{\partial x_i}\right)+\lambda\left(\frac{\partial u_k}{\partial x_k}\right)\delta_{ij}. \tag{7}$$

Here, from the local thermodynamic equilibrium state of fluid, viscous coefficients, λ, μ satisfy the Stokes hypothesis, $3\lambda+2\mu=0$. And, energy terms of viscous flux are represented as follows:

$$\begin{aligned}(e_v)_5&=u\tau_{xx}+v\tau_{xy}+w\tau_{xz}+\frac{\mu}{(\gamma-1)\mathrm{Pr}}\frac{\partial c^2}{\partial x},\\ (f_v)_5&=u\tau_{yx}+v\tau_{yy}+w\tau_{yz}+\frac{\mu}{(\gamma-1)\mathrm{Pr}}\frac{\partial c^2}{\partial y},\\ (g_v)_5&=u\tau_{zx}+v\tau_{zy}+w\tau_{zz}+\frac{\mu}{(\gamma-1)\mathrm{Pr}}\frac{\partial c^2}{\partial z}.\end{aligned} \tag{8}$$

To complete the set of compressible equations, the perfect gas equation of state is defined as

$$p=\rho(\gamma-1)\left\{e-\tfrac{1}{2}(u^2+v^2+w^2)\right\}, \tag{9}$$

where γ represents the specific heat ratio.

The solution algorithm is based on the PISO method,[13] and the fully implicit scheme[14] is used for time discretization and the quadratic upstream interpolation for convective kinematics (QUICK) scheme[15] is used for spatial discretization. The QUICK scheme is a higher order differencing scheme, and uses a three point upstream weighted quadratic interpolation for cell face values. The formulation of the QUICK scheme for uniform grid spacing is given by following expression:

$$\begin{aligned}f_r&=\tfrac{1}{2}(f_i+f_{i+1})-\tfrac{1}{8}(f_{i+1}-2f_i+f_{i-1}),\\ f_l&=\tfrac{1}{2}(f_i+f_{i-1})-\tfrac{1}{8}(f_i-2f_{i-1}+f_{i-2}).\end{aligned} \tag{10}$$

Based on an analysis of the truncation error the properties of the QUICK scheme for $\partial f/\partial x$ can be expressed as

$$\left.\frac{\partial f}{\partial x}\right|_i=\frac{f_r-f_l}{\Delta x}. \tag{11}$$

In the numerical simulation of the piston/sliding-door/cavity geometry, an additional equation called the geometric conservation law[16] (GCL) is solved for the moving coordinate velocity. The integral form of GCL is derived from the conservation of mass by setting the density of fluid, $\rho=1$ and the velocity of fluid flow, $v=0$. It can be written as follows:

$$\frac{d}{dt}\int_V dV=\int_S \mathbf{u}_s\cdot dS, \tag{12}$$

where $\mathbf{u}_s$ represents the local velocity of cell boundary, V is the volume of element, and S is the surface area of element. Equation (12) means that the change in volume of each control volume between two time instants, t^n and t^{n+1}, must be equal to the volume swept by the cell boundary during that time $\Delta t=t^{n+1}-t^n$. By a transformation from the Cartesian coordinate (x,y,z) to the body-fitted coordinate (ξ,η,ζ), the following form of the integral statement is acquired:

$$\frac{d}{dt}\int_V Jd\xi d\eta d\zeta=\int_V(\nabla\cdot\mathbf{u}_s)Jd\xi d\eta d\zeta. \tag{13}$$

Here, J represents the volume element in the transformed coordinate. Therefore, the computed value of J must be consistent with the value of ΔV implied by the numerical scheme used for solving the flow equation. Expanding the right-hand side of Eq. (13) and after performing necessary manipulations, the following form of the differential statement of GCL is obtained:

$$J_t+(\xi_t)_\xi+(\eta_t)_\eta+(\zeta_t)_\zeta=0, \tag{14}$$

where, ξ_t, η_t, ζ_t are the metric terms given by

$$\begin{aligned}\xi_t&=-[\dot{x}(y_\eta z_\zeta-y_\zeta z_\eta)+\dot{y}(z_\eta x_\zeta-z_\zeta x_\eta)+\dot{z}(x_\eta y_\zeta-x_\zeta y_\eta)],\\ \eta_t&=-[\dot{x}(y_\zeta z_\xi-y_\xi z_\zeta)+\dot{y}(z_\zeta x_\xi-z_\xi x_\zeta)+\dot{z}(x_\zeta y_\xi-x_\xi y_\zeta)],\\ \zeta_t&=-[\dot{x}(y_\xi z_\eta-y_\eta z_\xi)+\dot{y}(z_\xi x_\eta-z_\eta x_\xi)+\dot{z}(x_\xi y_\eta-x_\eta y_\xi)].\end{aligned} \tag{15}$$

Here, $\dot{x}$, $\dot{y}$, $\dot{z}$ are the grid velocities in the x, y, and z directions, respectively. Equation (14) is solved numerically to update the Jacobian values at each time step. The difference equation for the fully implicit scheme is given by

$$J^{n+1}=J^n-\Delta t[(\xi_t)_\xi^{n+1}+(\eta_t)_\eta^{n+1}+(\zeta_t)_\zeta^{n+1}], \tag{16}$$

where the metric coefficients are calculated from Eq. (15) at the $(n+1)$th time step and the grid velocities are calculated as follows:

$$\dot{x}^{n+1}=\frac{x^{n+1}-x^n}{\Delta t},\quad \dot{y}^{n+1}=\frac{y^{n+1}-y^n}{\Delta t},\quad \dot{z}^{n+1}=\frac{z^{n+1}-z^n}{\Delta t}. \tag{17}$$

C. Kirchhoff integral method and method of images

The Kirchhoff integral method applies the wave equation between a known acoustic surface, S, and a point in space within a uniform field.[17] The surface is assumed to contain all nonlinear flow effects and noise sources. This method allows propagation of a known sound field to a single point in space, and is useful when acoustic near field is already known.

The linear Kirchhoff integral formula is as follows:

$$p'(\vec{x},t) = \frac{1}{4\pi}\int_S \int \left[\frac{\cos\theta}{r^2}p' - \frac{1}{r}\frac{\partial p'}{\partial n} + \frac{\cos\theta}{cr}\frac{\partial p'}{\partial \tau} \right] \times dS(\vec{y},\tau). \tag{18}$$

Here, p' is the perturbed pressure, $(\vec{x},t)$ are the observer's location and time, $(\vec{y},\tau)$ are the source location and retarded time variables, θ is the angle between the normal vector $(\vec{n})$ on the surface and the radiation vector $(\vec{r})$, and r is the distance between an observer and a source at the retarded time. Note that pressure and its derivatives are calculated at the retarded time, τ.

To consider the road surface effect the method of images can be applied in the Kirchhoff integral formula.[11] Suppose that the mean flow is zero and let V be the region $y_2 \geqslant 0$ (shown in Fig. 4). It is constructed that the free space Green's function whose normal derivative vanishes on the boundary $y_2=0$. Since

$$G^0(\mathbf{y},\tau|\mathbf{x},t) = \frac{1}{4\pi R}\delta\left(\tau - t + \frac{R}{c_0}\right) \tag{19}$$

is a solution to the homogeneous wave equation when $\mathbf{y} \neq \mathbf{x}$, and since this equation is invariant under the transformation $y_2 \rightarrow -y_2$, a solution of the homogeneous wave equation that satisfies the causality condition is

$$h = \frac{1}{4\pi R'}\delta\left(\tau - t + \frac{R'}{c_0}\right), \tag{20}$$

where $R' = |\mathbf{x}-\mathbf{y}'|$ and $\mathbf{y}' = y_1\mathbf{i} - y_2\mathbf{j} - y_3\mathbf{k}$. Then, as $\mathbf{y}'$ is never in V, h is nonsingular in this region, the Green's function satisfies the boundary condition of the road surface in the region V is

$$G(\mathbf{y},\tau|\mathbf{x},t) = \frac{1}{4\pi R}\delta\left(\tau - t + \frac{R}{c_0}\right) + \frac{1}{4\pi R'}\delta\left(\tau - t + \frac{R'}{c_0}\right). \tag{21}$$

IV. PREDICTION OF AIR-PUMPING NOISE

The tire is modeled as a cylindrical geometry which has the dimension of 165/70 SR 13 tire and the traveling speed is 100 km/h (27.8 m/s). Thus, it has a dimension of 346.64 mm in radius ($0.5D$) and a width (W) of 165 mm. The contact patch length is assumed to be 189 mm, which is reported in previous experiment[18] in case of the tire being loaded by two passengers. In addition, the tread pitch of the tire is adjusted to 55.6 mm so that the fundamental tread impact frequency at the speed of 100 km/h is 500 Hz. The tire groove is assumed to be a hexahedral cavity which has a dimension of 6 mm in width (w), 6 mm in depth (d), and 165 mm in length (l). In Fig. 5, the schematic diagram of the tire groove geometry is shown. The tire groove is assumed to be a transverse pocket-type where all sides of the hexahedral cavity are closed except for one open end. Moreover, in order to consider the relative motion of the contact patch, the sliding door is located at the open end. The adoption of the transverse pocket-type groove has an advantage in investigating the nonlinearity of the air-pumping noise generation mechanism through the reduction of the air flow in the direction of tire side-wall. As reported in previous research,[19] the decrease in volume of the tire groove is assumed to be 10% of the total volume. In addition, the volume changes are assumed to be simple harmonic. The dimensions and numerical settings are listed in Table I.

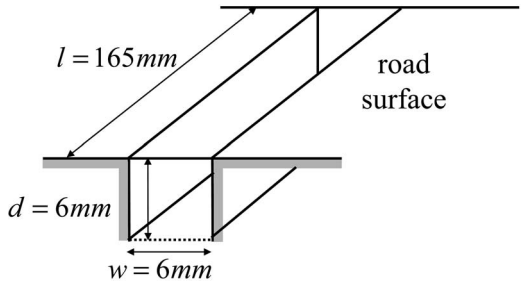

FIG. 5. Schematic diagram of the tire groove geometry (transverse pocket-type groove).

As mentioned earlier, when the monopole theory is applied to predict the air-pumping noise, directional characteristics of the air-pumping noise and the geometrical effects on noise generation and propagation cannot be investigated. Instead of using the monopole theory, therefore, the linear source model which equates the air movement exactly with the volume changes of the tire groove is introduced. Through the comparison of the linear and the nonlinear source model, the nonlinear characteristics of the air-pumping noise are investigated. In case of predicting air-pumping noise with the linear source model, the air velocity at the open end of the cavity is assumed to be identical to the velocity of the piston. In addition, the air density is to be constant in ambient value. Therefore, the input in numerical simulation of the full tire/road domain is acquired in algebraic manner and a numerical simulation of small-scale noise generation is not necessary.

TABLE I. Dimensions and numerical settings.

Tire radius (165/70 SR 13)	346.64 m
Adjustment of the tread pitch	55.6 mm
Car speed	100 km/h (27.8 m/s)
Contact patch length	189 mm
Tread passing frequency	500 Hz
Cavity compression/expansion period (T_p)	0.000 215 83 s
Total air-pumping period (T)	0.002 s
Total volume change	$165\times6\times0.6\times10^{-9}=594\times10^{-9}$ m^3
Variation of cavity depth in compression process	$d-d\times0.1\times\{\frac{1}{2}\times(1-\cos(\pi t/T_p))\}$

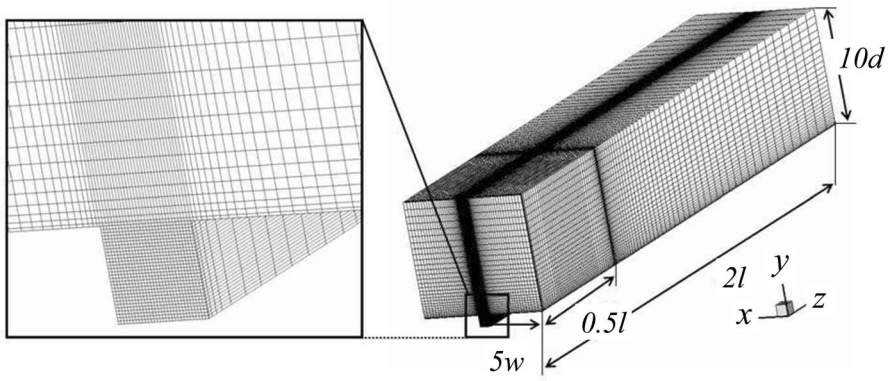

FIG. 6. Computational mesh for the simulation of the piston/sliding-door/cavity source model.

A. Small-scale noise generation simulation

The small-scale air-pumping noise generation process modeled with the piston-sliding-door/cavity geometry is numerically simulated. The grid system is characterized by a hexahedral free field domain and a cavity domain, which represents the tire groove. Figure 6 shows the computational mesh for the air-pumping noise source model simulation. The free field domain has a dimension of 10w in width, 10d in depth, and 2l in length. Total number of nodes is 406 172 and total number of cells is 384 000. In order to separate the air-pumping noise source to the turbulent noise source, it is assumed that there is no mean flow. Besides, the road surface is assumed to be perfectly reflective. Therefore, no-slip boundary condition is imposed at the cavity surfaces, the sliding-door surface, and the road surface. For the reduction of computational cost, a symmetric boundary condition is taken on the tire's plane of symmetry and the flow analysis is performed in a half of the tire groove.

Figure 7 shows the contours of the perturbed pressure in the air-pumping noise generation process. Each sectional diagram shows the perturbed pressure distributions on the planes parallel to the XY plane, located at distances 20, 40, 60, and 80 mm from the tire's plane of symmetry. Also, Fig. 8 shows streamlines on the tire's plane of symmetry.

At the contact patch leading edge, the cavity is gradually covered by the sliding-door and, at the same time, the air in it is compressed by the piston. Thus, the air flow in the cavity evacuates with a bias, and a vortical flow is generated outside the cavity. This vortical motion of the evacuating flow is suppressed by the road surface in real situation and by the wall boundary condition in the second stage flow simulation of the full tire/road domain. However, at the contact patch trailing edge, there exists a vortical flow in the cavity rather than the outside it. This vortical flow generation in the tire groove results from the collision of the compressed outgoing air flow and the incoming air flow suctioned by the piston. Judging from a standpoint of the monopole theory, therefore, the compressed air suppresses the volume increase of noise source. Thus, it is expected that the characteristics of the air-pumping noise are not harmonic even if the volume changes of the cavity are. That is to say, the compressibility of air and the relative motion of road surface to the tire groove will cause the difference between the spectral characteristics of air-pumping noise and that of noise source.

In addition, as seen in Fig. 7, even though the tire has transverse pocket-type grooves, there exists an air flow around the tire sidewall, or near the side of the cavity. The air is compressed and pressed away to this region at the contact patch leading edge, and expanded and sucked into the cavity from it at the contact patch trailing edge. Therefore, this perturbed pressure around the tire sidewall region will generate the far field air-pumping noise in this direction. However, in case of using the linear source model, even in the Helmholtz resonance approach, this air flow cannot be taken into account due to the assumption of equating air velocity to that of the moving piston.

B. Near-field noise propagation simulation

In the second stage, the unsteady flow data acquired by the small-scale noise generation simulation are used as air-pumping noise sources in the near-field noise propagation simulation with the full tire/road geometry. In Fig. 9, the computational mesh for the full tire/road geometry is shown. The computational domain has a dimension of 10D in radius and 10W in width. Total number of nodes is 250 650 and total number of cells is 240 044. As the piston/sliding-door/cavity simulation, a pressure prescribed boundary condition is applied at far boundary and a symmetric boundary condition is taken on the tire's plane of symmetry. A no-slip boundary condition is imposed on the tire and the road surface, which is adjusted by the angular velocity of the tire for the cylinder wall and the traveling speed for the road surface.

Figures 10 and 11 show the results of the simulation of the full tire/road domain with the linear source model (model 1) and with the proposed piston/sliding-door/cavity model (model 2), respectively. First, it is found that the tire/road geometry has an effect on not only the air-pumping noise generation process but also the air-pumping noise propagation. As the compression waves which are generated by the air-pumping noise sources at the contact patch edges propagate through the hornlike region, wave fronts are deformed normal to the surfaces around the tire and the road. This wave front deformation is observed both two model cases. Thus, it is inferred that the cause of this deformation of the wave form is not the nonlinear characteristics of the air-pumping noise generation mechanism but the horn-like geometry.

Though the geometrical effect is observed in both two model cases, it is easily seen the difference between model 1

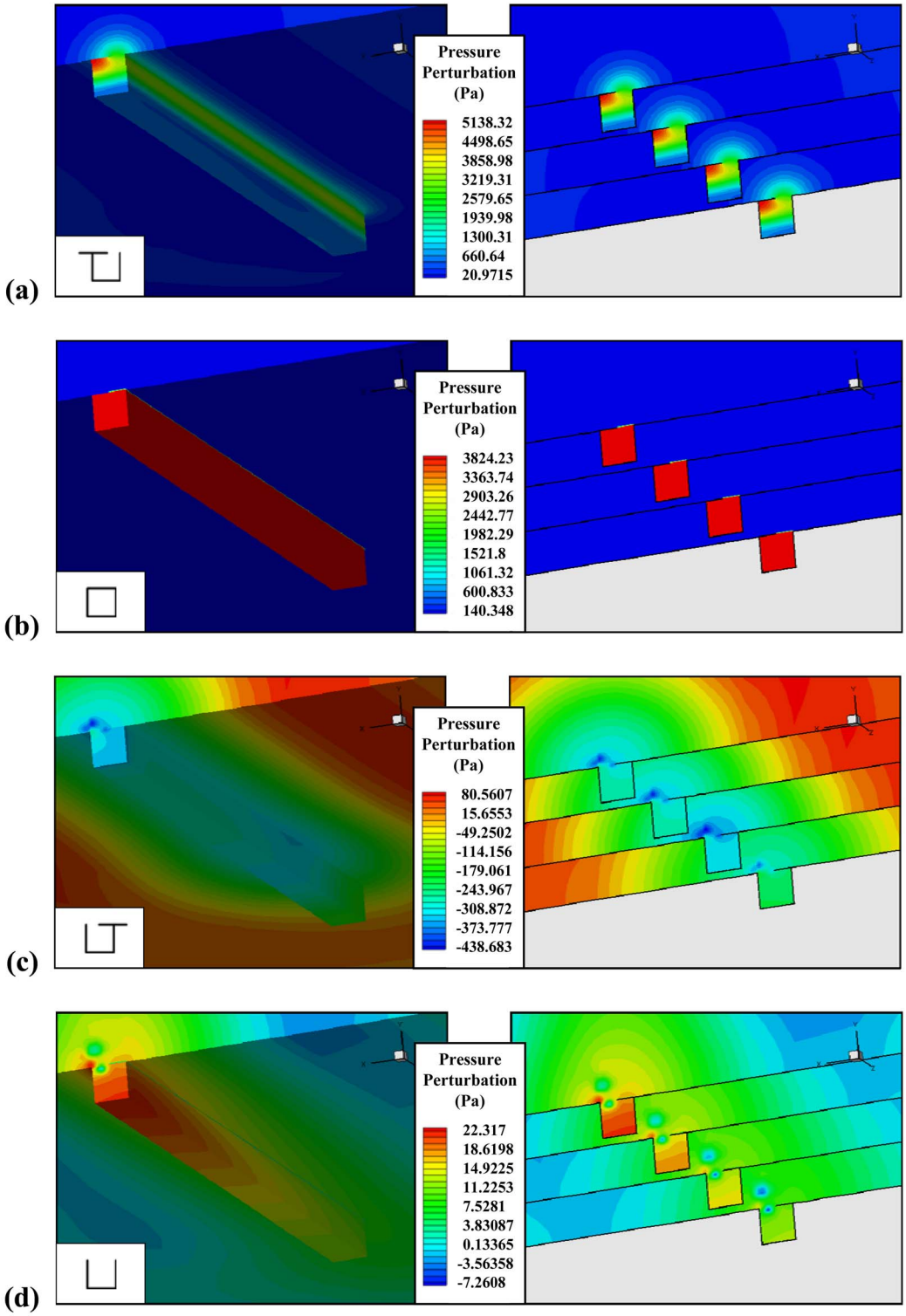

FIG. 7. (Color online) Pressure perturbation contours of the nonlinear (piston/sliding-door/cavity) source model in air-pumping noise generation process at (a) $t=T_p/2$ (contact patch leading edge), (b) $t=T$ (contact patch leading edge), (c) $t=T_p/2$ (contact patch trailing edge), and (d) $t=T$ (contact patch trailing edge).

and model 2. In case of model 1, the perturbed pressure is distributed almost uniformly along the tread area of the tire and weak pressure perturbation is observed on the tire sidewall. However, in case of model 2, at the initial stage of air-pumping, there exists a strong pressure perturbation near the tire sidewall, especially around the contact patch leading and trailing edge. This pressure perturbation on the tire sidewall is due to the air flow in the region of the side of the tire groove, which is observed in Fig. 7. As mentioned before, the pressure perturbation in the region of the tire side-wall will cause the far-field noise propagation in the direction of the side of a rolling tire and, as a result, the different directivity pattern from that of the air-pumping noise with the linear source model.

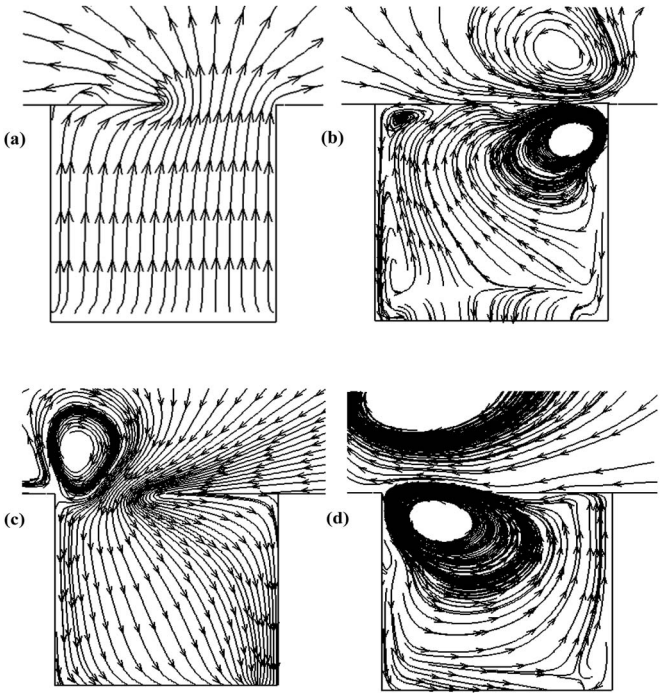

FIG. 8. Streamlines on the plane of symmetry of the tire at (a) $t=T_p/2$ (contact patch leading edge), (b) $t=T$ (contact patch leading edge), (c) $t=T_p/2$ (contact patch trailing edge), and (d) $t=T$ (contact patch trailing edge).

C. Far-field acoustic pressure prediction

The far-field acoustic pressure is predicted by use of the Kirchhoff integral formula with the near-field flow data obtained in the second stage. In the present study, the cylindrical surface which is magnified the tire surface five times is considered as the control surface. In addition, to consider perfectly reflective ground surface, the image sources of sound are imposed under the road surface.

Figure 12 shows the predicted acoustic pressure variations for several angles from the direction of travel during one air-pumping period at the position 7.5 m distance from the origin of the tire, the measurement point recommended in ISO R 362. From Eq. (5), the predicted acoustic pressure by use of the monopole theory is given by

$$p'(r,t) = \frac{1}{4\pi r}\rho_0 \frac{\partial^2 V}{\partial t^2}\left(t - \frac{r-a}{c}\right)$$

$$\approx 1.0772 \cos(14556t - 318.28)\ \text{Pa}. \qquad (22)$$

Because the monopole theory models the air-pumping noise source as a point monopole source, the anti-phasic behavior of the air-pumping noise sources at the contact patch leading and trailing edges is not considered. Further, the cancellation process through the acoustic reflection by the tire and the road surfaces is not taken into account, either. Therefore, the predicted acoustic pressure level of the monopole theory is higher than that of the proposed method, which is shown in Fig. 12.

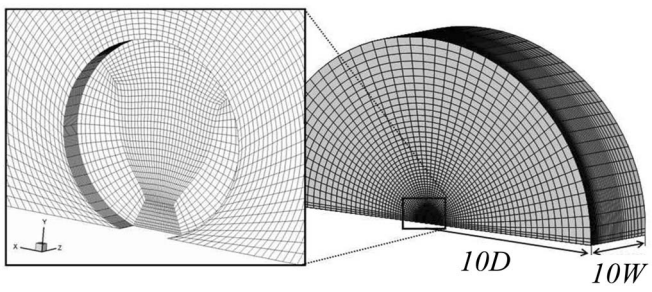

FIG. 9. Computational mesh for the simulation of the full tire/road domain.

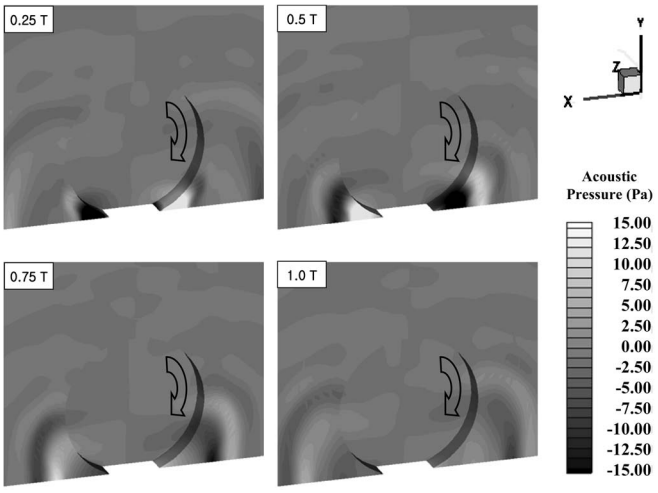

FIG. 10. Pressure perturbation contours of the full tire/road domain simulation with the linear source model in air-pumping noise generation process at (a) $t=T/4$, (b) $t=T/2$, (c) $t=3T/4$, and (d) $t=T$.

By comparison between the time history of the air-pumping noise generated with the linear source model (model 1) and that with the nonlinear source model (model 2), the nonlinear characteristics of the air-pumping noise can be ascertained. In case of model 1, the acoustic pressure amplitude has a symmetric distribution to the *YZ* plane (the axis of rotation of the tire, 90° Fig. 12) and its phase has an antisymmetric distribution. Moreover, there is little acoustic propagation in the direction of the axis of rotation of the tire. However, in case of model 2, contrary to the case of model 1, noise propagation in the direction of the axis of rotation of

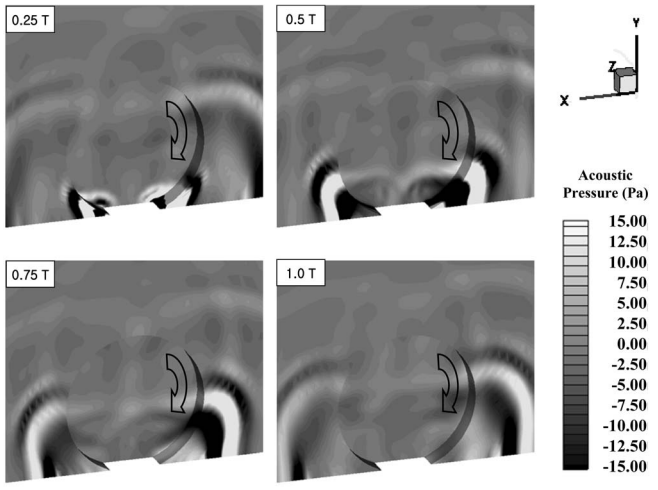

FIG. 11. Pressure perturbation contours of the full tire/road domain simulation with the nonlinear (piston/sliding-door/cavity) source model in air-pumping noise generation process at (a) $t=T/4$, (b) $t=T/2$, (c) $t=3T/4$, and (d) $t=T$.

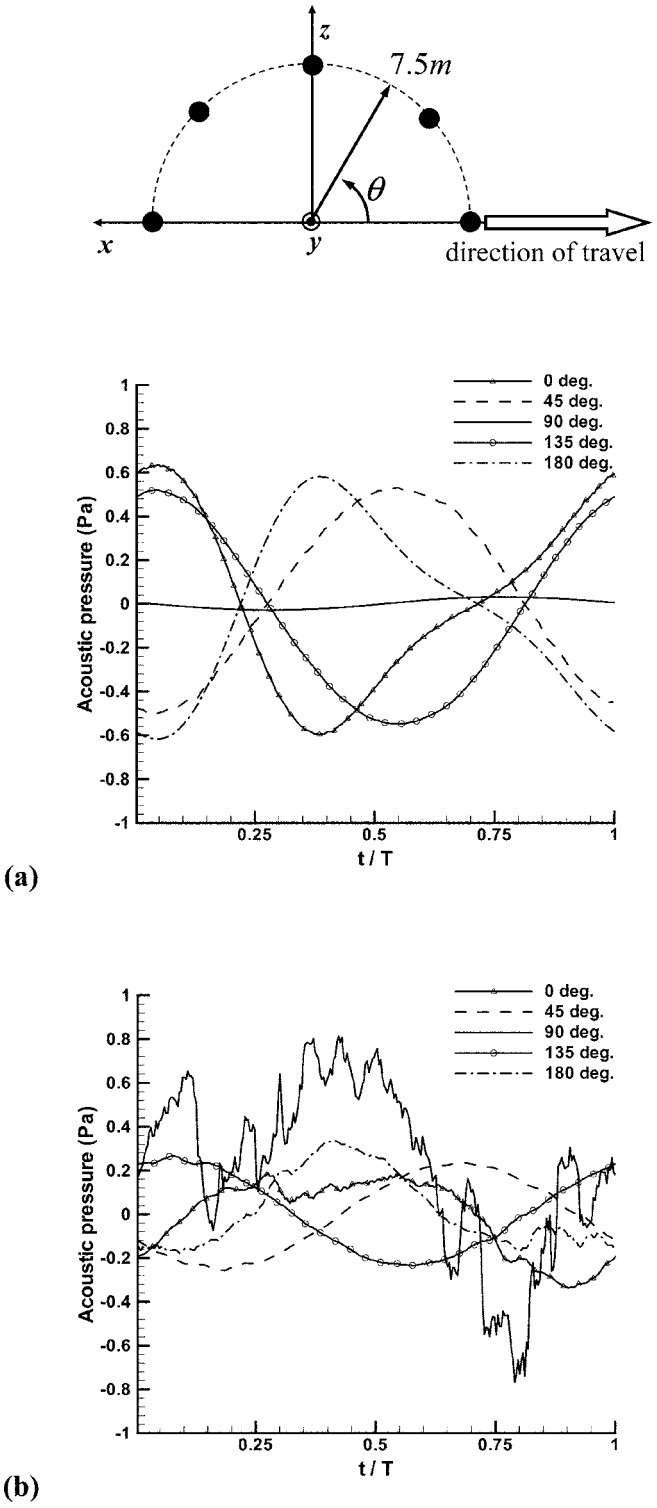

FIG. 12. Predicted acoustic pressure variations at the position 7.5 m distance from the origin of the tire (z=7.5 m) with (a) the linear noise source model and (b) the nonlinear (piston/sliding-door/cavity) source model during one period of air-pumping.

the tire is dominant. In addition, the level of the acoustic pressure of model 2 in the direction of travel of the tire (0° or 180°) is slightly lower than that of model 1. It seems that this disparity between model 1 and 2 results from the nonlinear behavior of the air-pimping noise source. In case of model 1, the phases of the air-pumping sources behavior at the contact patch leading and trailing edges are perfectly anti-phase each other. In addition, the nonmoving tire road geometry is symmetric to the axis. As a result, there exists a strong cancellation in the direction of the axis of rotation of the tire where retarded times from the contact patch leading edge and that from the trailing edge are nearly same each other. Thus, the level of the air-pumping noise is gradually decreasing as the observation point moves from the direction of travel (0° or 180°) to the direction of the axis of rotating of the tire (90°). But, in case of model 2, as mentioned before, the compressed air in the cavity is pressed away at the beginning of expansion process and interrupts suction of outside air into the cavity. Therefore, the phases of the air-pumping sources behavior at the contact patch leading and trailing edges are not perfectly anti-phase each other. Thus, there exists a weak cancellation. In addition, as seen in Fig. 7, a strong pressure perturbation is generated in the region of the side of the tire groove, or near the tire side-wall. Thus, this pressure perturbation may increase the noise propagation in the direction of the axis of rotation of the tire. Similar result is shown in the ISO-sound-intensity contour diagrams for crossbar tread tire on smooth surface reported in the experimental data by Donovan and Oswald.[20] The experimental data shows that the acoustic intensity level in the tire side-wall area (in the direction of the axis of tire rotation) is significant, although not as high as that at the contact patch leading edge region.

In order to investigate the directivity pattern of the air-pumping noise more clearly, the acoustic pressure distribution on the surface which has a radius of 7.5 m from the origin of the tire is shown in Fig. 13. As seen in Fig. 12, in case of the linear source model, the directivity patterns have an antisymmetric configuration to the *YZ* plane. Whereas, in case of the nonlinear source model, it is apparently seen that the noise radiation toward the direction of the axis of rotation of the tire is dominant and the level of the air-pumping noise in the forward direction is higher than that in the backward direction. This forward directivity results from the relative motion of the road surface to the tire groove and the compressibility of air. At the contact patch leading edge, the closing movement of the sliding-door (i.e., road surface) helps the air in the tire groove compressed more highly. At the contact patch trailing edge, however, the compressed air in the tire groove and the opening movement of the sliding-door prevent the tire groove from sucking the outside air. Therefore, the noise emission of the air-pumping sources at the contact patch leading edge becomes more efficient. Similar forward directivity is shown in the intensity level contour diagrams reported in the Technical University of Gdansk experimental data.[2] The experimental data show that the high-emission region locates at the leading edge of the footprint in the sound intensity maps for a summer tire tested at 90 km/h on a very smooth surface for frequency within the range 1000–3150 Hz, which is the generally reported frequency range of the air-pumping noise.

In order to investigate the characteristics of the air-pumping noise in frequency domain, the spectral analysis is performed with the acoustic pressure time history which is presented in Fig. 12. In Fig. 14, the predicted A-weighted air-pumping noise spectrum which is generally used in the measurement of the tire/road noise is presented at one-third

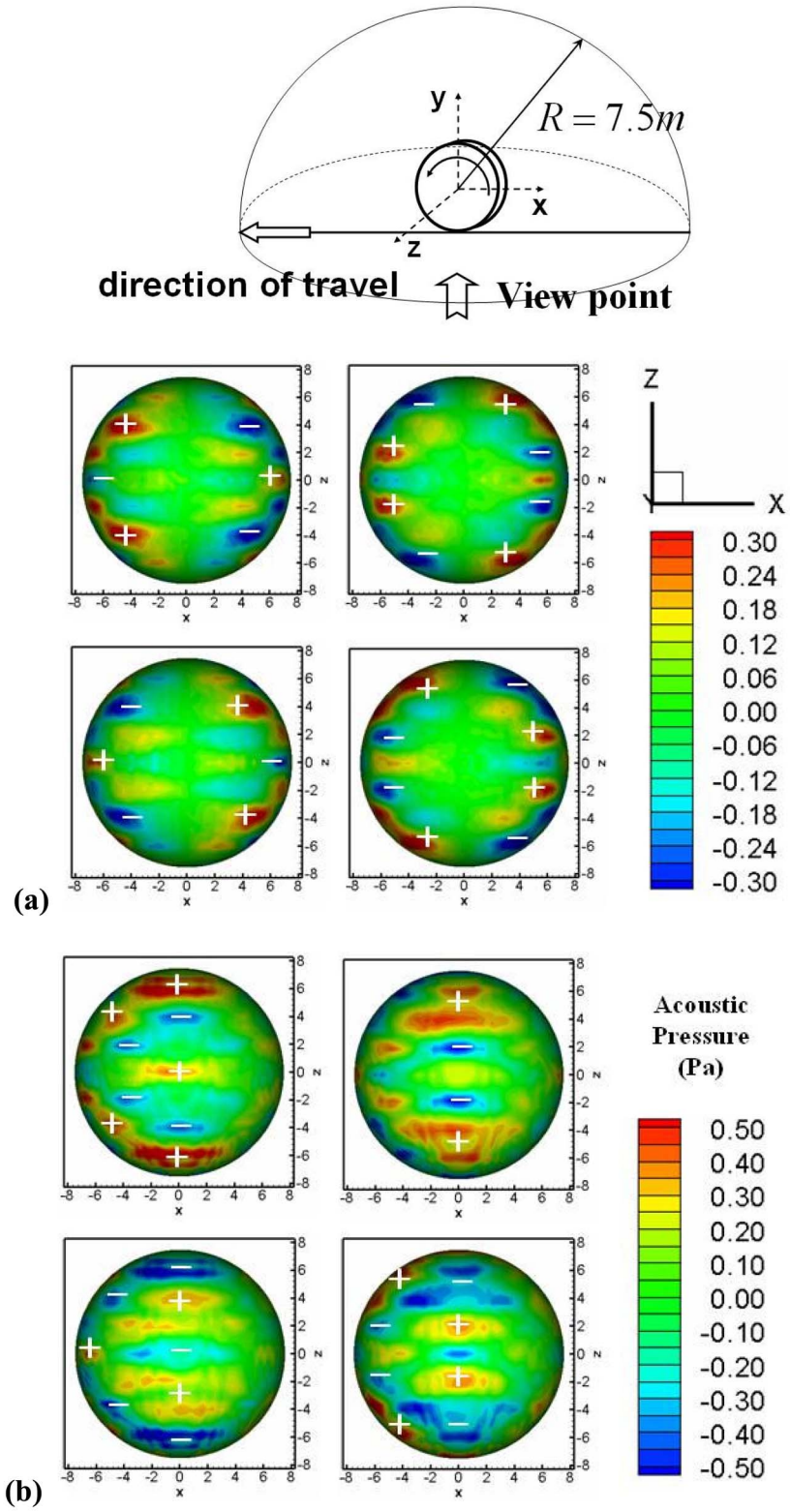

FIG. 13. (Color online) Predicted acoustic pressure distribution with (a) the linear noise source model and (b) the nonlinear (piston/sliding-door/cavity) source model during one period of air-pumping.

octave band frequencies. In the present study, the tread pattern periodicity was 55.6 mm, giving an expected excitation frequency of 500 Hz, which also appears in the spectra as a peak in both model cases. However, in case of model 2, the second peak at frequency approximately 1 kHz has a higher level than that of model 1. This higher level of the second peak frequency seems to result from the pipe resonance of the tire groove. The resonance frequency of the air in a pipe closed in both end is given by

$$f_r = \frac{c}{2l}, \tag{23}$$

where f_r is the resonance frequency (Hz), c is the speed of sound (m/s), and l is the length of the pipe (m). In the present study, the pipe resonance frequency is 1039.39 Hz. Thus, it is shown that the pipe resonance effect is predictable in case of model 2 in which the air-pumping noise source is modeled with the piston/sliding-door/cavity geometry and

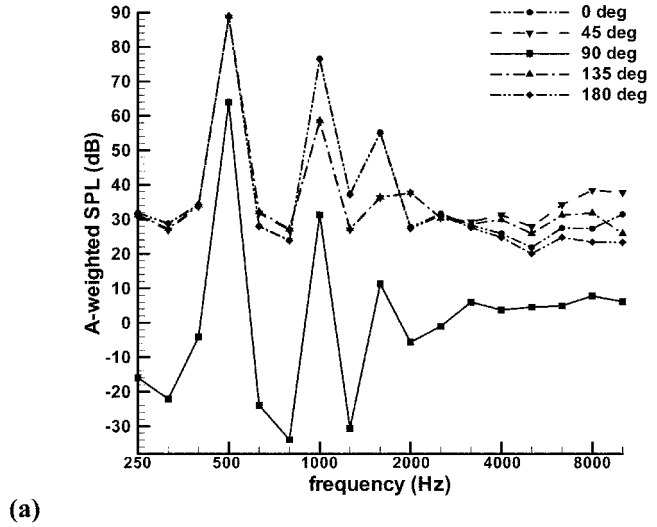

FIG. 14. Predicted A-weighted air-pumping noise spectra with (a) the linear noise source model and (b) the nonlinear (piston/sliding-door/cavity) source model at one-third octave band frequencies.

numerically simulated. Further, in case of model 2, the predicted noise levels within the range 2–8 kHz where it is reported that the air-pumping noise has most of its energy concentrated are increased, especially in the direction of the axis of rotation of the tire (90°). As mentioned before, the increase of noise emission in this direction is caused by the strong pressure perturbation near the tire sidewall, which results from the compressibility of the air and the relative motion of the road surface to the tire groove. Therefore, it is expected that the consideration of the nonlinear effect will be indispensable to study air-pumping noise generation and propagation.

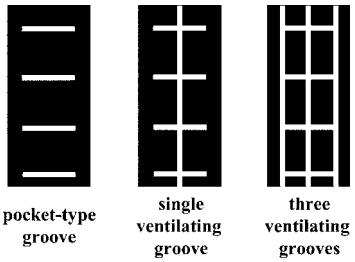

FIG. 15. Experimental tread patterns used in the study of the influence of pocket groove (Ref. 4).

V. INFLUENCE OF VENTILATION ON AIR-PUMPING NOISE

The air-pumping mechanism is believed to be one of the most important in tire/road noise generation and many researches for investigating the air-pumping noise generation mechanism are in progress. However, the tire/road noise generation mechanism is an extremely complicated mixture of dynamic mechanisms and related phenomena, so it is difficult to identify the air-pumping noise. Furthermore, there are few research results that can be quantitatively compared with the predicted result in the present study. Therefore, to validate the proposed method, predicted results are qualitatively compared with experimental results of the influence of the pocket-type grooves on air-pumping noise spectra performed by Ejsmont *et al.*[4] In their experiment, the influence of pockets in the tread was observed on a hand-cut experimental tire. The tread patterns used in the experiment are shown in Fig. 15. In their experiment the tire geometry, the traveling speed of the tire, and the tread pitch are same as the numerical settings of the present study. The length and depth of the experimental tire groove are not reported, however, so the tire groove is assumed to have the same dimension as that of the present study. In addition, the ventilating cavity would have the dimension as the tire groove width and a half of the tire groove depth. In Fig. 16, the schematic diagram of the ventilated piston/sliding-door/cavity source model is shown. In order to ventilate the tire groove, an additional hexahedral

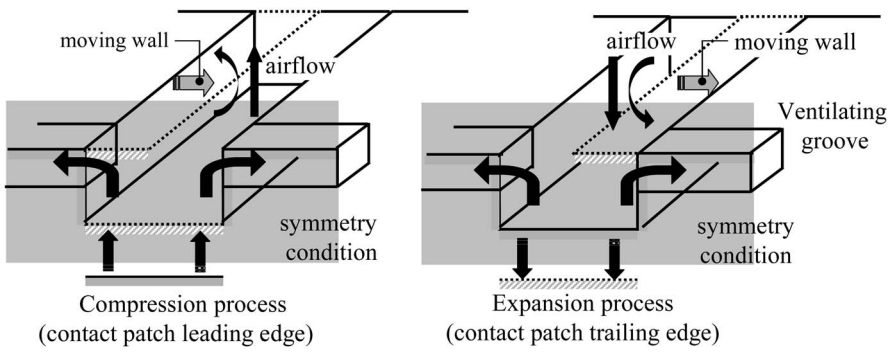

FIG. 16. Schematic diagram of the ventilated piston/sliding-door/cavity source model.

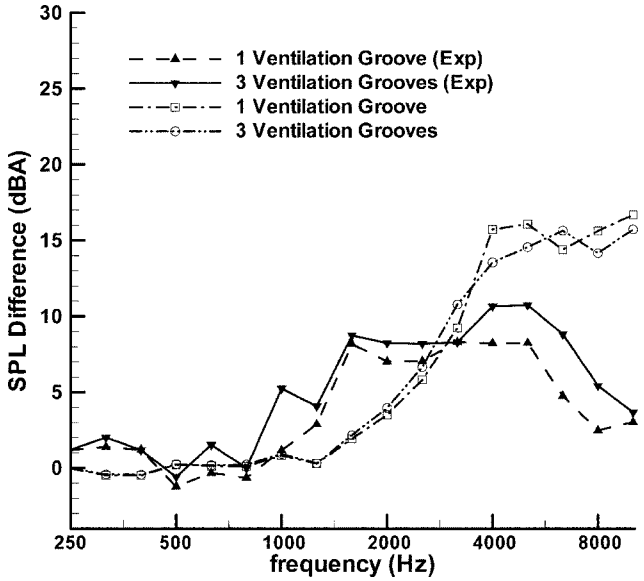

FIG. 17. Influence of the ventilating pocket-type groove on air-pumping noise spectrum. SPL difference between pocket type groove and ventilated pocket type groove at one-third octave band frequencies at the position 62.82° from the direction of travel on *XZ* plane.

cavity adjacent to the original piston/sliding-door/cavity model is equipped. As a result, though the tire groove is closed by the sliding-door in the air-pumping process, the air compressed by the piston can evacuate through the ventilating cavity.

Figure 17 shows the SPL difference between the pocket type groove and the ventilated pocket type groove at one-third octave band frequencies at the position 62.82° from the direction of travel on *XZ* plane. In the experimental result, the ventilation of the pockets by circumferential groove decreases the levels of frequencies within the range 2–6.5 kHz. However, the decrease of the predicted noise level occurs for frequencies within the range 3–8 kHz. This discrepancy in frequency range seems results from the difference of the tire groove and the ventilating groove geometry with the experimental tire. Even though the discrepancy is somewhat large in the low frequency domain, it shows that the predicted results showing a decreasing tendency of the noise levels at frequencies affected by the nonlinearity of air-pumping noise agree well with the experimental results. Through experimental results of the influence of the groove width[4] which has a nonlinear dependence of emitted sound intensity upon it, the groove width has been found to have dominant effects on the air-pumping noise level at the frequencies about 1–4 kHz. Meanwhile, as seen in Fig. 14, the frequency range in which the noise level is affected by the nonlinearity of the air-pumping noise is about 2–8 kHz in the present study. Thus, it can be inferred that the ventilation of the pocket-type groove has dominant effects on the noise sources which have nonlinear characteristics, and it can be checked in both experimental and predicted results.

Further, it is also found in both cases that a single ventilating groove eliminates the air-pumping noise level, which has nonlinear characteristics, almost as much as by three ventilating grooves.

VI. CONCLUDING REMARKS

In order to investigate the air-pumping noise from a car tire, a novel method based on a hybrid technique that combined a CFD technique with a Kirchhoff integral method is proposed. The air-pumping noise source behavior is obtained by the small-scale noise generation simulation with the piston/sliding-door/cavity model, which takes into account the relative motion of the road surface to the tire in the air-pumping noise generation process. The obtained flow properties in the tire grooves are then transferred to the flow simulation of the full tire/road domain as an air-pumping noise source. Finally, the far-field acoustic pressure is predicted by the linear Kirchhoff integral method through the use of the acquired flow properties around rolling tire and road surface geometry.

Through the comparison of the linear and the nonlinear source model simulations, it is found that the nonlinearity of the air-pumping noise source affects not only noise characteristics in frequency domain but also in the directivity pattern. While the sound field of the linear air-pumping source is symmetric to the axis of rotation of the tire, the directivity pattern of the nonlinear air-pumping source is asymmetric, i.e., the nonlinearity of the air-pumping noise source increases the emission of noise in the direction of the axis of rotation and in the direction of traveling of the tire. In the frequency domain, it is found that an increase in noise emission occurs for frequencies within the range of 2–8 kHz where it is reported that the air-pumping noise has most of its energy concentrated. Further, through a qualitative comparison of the ventilating effect with the measured data, it is also found that this noise peak level at frequencies 3–8 kHz is suppressed by a ventilation of the tire groove. It shows that the predicted results showing a decreasing tendency of the noise levels at frequencies affected by the nonlinearity of air-pumping noise agree well with the experimental results.

By use of the three-stage hybrid technique based on a numerical method with nonlinear governing equations, the proposed prediction method can take into account the effect of the tire/road geometry and the nonlinearity of the air-pumping noise source. Thus, the proposed method can cover the important physical processes of the air-pumping mechanism: the small-scale nonlinear noise generation, the mid-scale acoustic scattering process and the far-field noise propagation. From an engineering viewpoint, the proposed methodology is capable of providing us with an efficient method for further noise reduction and for the tire/road noise control.

ACKNOWLEDGMENT

This work was supported by Grant No. R01-2001-000-00401-0 from Korea Science and Engineering Foundation.

[1]M. Heckl, "Tyre noise generation," Wear **113**, 157–170 (1986).
[2]J. A. Ejsmont and U. Sandberg, *Tyre/Road Noise Reference Book* (INFOMAX, Harg, SE-59040 Kisa Sweden, 2002).
[3]R. E. Hayden, "Roadside noise from the interaction of a rolling tire with road surface," in Proceedings of the Purdue Noise Conference, West Lafayette, IN, 1971, pp. 62–67.
[4]J. A. Ejsmont, U. Sandberg, and S. Taryma, "Influence of tread pattern on tire/road noise," in *Transactions of the Society of Automotive Engineers*

(Society of Automotive Engineers, Warrendale, 1984), pp. 1–9.
[5]M. Jennewein and M. Bergmann, "Investigations concerning tyre/road noise sources and possibilities of noise reduction," Proc. Inst. Mech. Eng., Part C: Mech. Eng. Sci. **199**, 199–205 (1985).
[6]M. J. Gagen, "Novel acoustic sources from squeezed cavities in car tires," J. Acoust. Soc. Am. **106**, 794–801 (1999).
[7]J. F. Hamet, C. Deffayet, and M. A. Pallas, "Air-pumping phenomena in road cavities," in International Tire/Road Noise Conference 1990, pp. 19–29.
[8]N. A. Nilsson, "Air resonant and vibrational radiation—possible mechanisms for noise from cross-bar tires," in International Tire/Road Noise Conference 1979, pp. 93–109.
[9]P. Guisset and F. Augusztinovicz, "TINO noise emission: Analysis and prediction models," in First International Colloquium on Vehicle Tyre and Road Interaction, Paper 99.06, 1999.
[10]B. B. Bakerand and E. T. Copson, *The Mathematical Theory of Huygens' Principle* (Clarendon, Oxford, 1953).
[11]M. E. Goldstein, *Aeroacoustics* (McGraw-Hill, New York, 1976).
[12]K. J. Plotkin and E. Stusnick, "A unified set of models for tire/road noise generation," Wyle Research Report No. WR 81–26, Wyle Laboratories, Arlington, 1981.
[13]R. I. Issa, "Solution of the implicitly discretised fluid flow equations by operator-splitting," J. Comput. Phys. **62**, 40–65 (1986).
[14]R. D. Richtmeyer and K. W. Morton, *Difference Methods for Initial-Value Problems*, 2nd Ed. (Wiley-Interscience, New York, 1967).
[15]B. P. Leonard, "A stable and accurate convective modeling procedure based on quadratic upstream interpolation," Comput. Methods Appl. Mech. Eng. **19**, 56–98 (1979).
[16]R. Kamakoti and W. Shyy, "Evaluation of geometric conservation law using pressure-based fluid solver and moving grid technique," Int. J. Numer. Methods Heat Fluid Flow **14**, 851–865 (2004).
[17]R. R. Mankbadi, *Transition, Turbulence, and Noise: Theory and Applications for Scientists and Engineers* (Kluwer Academic, Boston, 1994).
[18]N. A. El-Sebai, M. Watany, and A. Saad, "Tire/road interface airborne noise characteristics generation," in *Proceedings of the 1999 Noise and Vibration Conference* (Society of Automotive Engineers, Warrendale, 1999), pp. 605–613.
[19]I. D. Wilken, L. J. Oswald, and R. Kickling, "Research on individual noise source mechanisms of truck tires: Aeroacoustic source," in *SAE Highway Noise Symposium* (Society of Automotive Engineers, Warrendale, 1976), 762024, pp. 181–186.
[20]P. R. Donovan and L. J. Oswald, "The identification and quantification of truck tire noise sources under on-road operating conditions," Research Publication No. GMR-3380, General Motors Research Laboratories, Warren, MI, 1980.